Nonperturbative time-dependent density-functional theory of ionization and harmonic generation in OCS and CS_2 molecules with ultrashort intense laser pulses: Intensity and orientational effects

Emmanuel Penka Fowe and Andre D. Bandrauk*

Laboratoire de Chimie Théorique, Faculté des Sciences, Université de Sherbrooke, Quebec, Canada, J1K 2R1

(Received 16 December 2010; revised manuscript received 18 May 2011; published 16 September 2011)

Molecular high-order harmonic generation (MHOHG) and molecular orbital ionization rates are calculated for the nonsymmetric OCS and symmetric CS_2 molecules using numerical solutions of Kohn-Sham (KS) equations of time-dependent density functional theory in the nonlinear nonperturbative regime of laser-molecule interactions for different laser-molecule orientations and intensities. It is found that the ionization of inner-shell KS molecular orbitals contributes significantly to the ionization and MHOHG processes for intensities $I \geqslant 3.5 \times 10^{14}$ W/cm^2. Ionization rate maxima correspond to the alignment of maximum KS orbital densities with the laser pulse polarization instead of orbital ionization potentials. Furthermore, degeneracies of orbitals are removed as a function of laser-molecule angle, thus affecting ionization rates, the MHOHG spectra, and their polarizations, the latter allowing for identifying inner-orbital ionization.

DOI: 10.1103/PhysRevA.84.035402 PACS number(s): 33.20.Xx, 33.80.Rv, 33.80.Wz, 33.90.+h

We report in this paper the nonlinear nonperturbative response to short (few cycles) intense laser pulses of the nonsymmetric OCS and symmetric CS_2 molecules. The time-dependent density functional theory (TDDFT) Kohn-Sham (KS) equation for each occupied molecular orbital (MO) in these molecules was discretized in space using finite-difference (FD) grid techniques as reported earlier for CO_2 and other molecules [1,2]. We have used the Van Leeuwen and Baerends [3] potential (LB94), which introduces a gradient correction to the local density approximation exchange correlation so as to reproduce correctly the Coulomb asymptotic behavior of the potential. It reproduces KS MO negative energies [1,4,5] nearly equal to the ionization potentials (IP) obtained from photoelectron spectra, which are only accurately given normally by many-body Dyson orbitals [6]. The bond length has been set to its experimental [7–10] value, i.e., OCS bonds length are CS = 0.156 nm, CO = 0.1157 nm, and CS = 0.155 nm for CS_2, and these molecules are oriented along the z axis. The time-dependent ionization probability $P_{i,\sigma}(t)$ of an individual spin-orbital is calculated [2] as

$$P_{i,\sigma}(t) = 1 - N_{i,\sigma}(t), \tag{1}$$

where $N_{i,\sigma}(t) = \langle \psi_{i,\sigma}(r,t) | \psi_{i,\sigma}(r,t) \rangle$ is the time-dependent population (survival probability) of the i,σth spin population. The number of electrons inside the grid of volume V and remaining population are

$$N_{\text{bound}}(t) = \int_V d^3r\, n(r,t) \quad \beta(t) = \frac{\int_V d^3r n(r,t)}{\int_V d^3r n(r,0)} = e^{-\Gamma t}, \qquad \gamma(t_f) = 1 - \beta(t_f) \tag{2}$$

where $n(r,0) = 2\sum_i^{N_\sigma} |\psi_{i\sigma}(r,0)|^2$ is the total number of electrons in the initial state (without external field). The total ionization yield probability $\gamma(t_f)$, computed at the final time t_f of the propagation, is then obtained from the difference between initial and final probability $\beta(t_f)$ in Eq. (2) and tabulated in Table I for different laser-molecule angles θ and intensities.

The power spectrum of the dipole acceleration $\ddot{d}_z(t)$ in a given direction yields the predicted MHOHG spectra [11,12]

$$S_z(\omega) \propto |a(\omega)|^2 = \left| \int \left(\frac{d^2}{dt^2} d_z(t) \right) e^{i\omega t} dt \right|^2. \tag{3}$$

Recent work has shown that the most accurate method for generating the MHOHG spectra when dealing with molecular systems [5,11,12] is to calculate the dipole acceleration $\ddot{d}_z(t)$ from the exact time-dependent function according to Ehrenfest's theorem.

We have investigated the time evolution of some relevant KS orbitals illustrated in Fig. 1 for zero field. Three angular orientations of the molecular z axis with respect to laser polarization are considered: $\theta = 0^\circ$, 45°, and 90°. Results using two laser intensities ranging from lower 3.5×10^{14} to higher 1.4×10^{15} W/cm^2 are displayed in Fig. 2(a) for the CS_2 molecule and in Fig. 2(b) for the OCS molecule. Evidence of a strong dependence of the KS remaining orbital population $N_{i,\sigma}(t)$ with the laser intensity is observed. It emerges as expected that, in general, the KS MO ionization is most important for CS_2 due to its lower IP as compared to OCS. When $\theta = 0^\circ$ (laser and molecule parallel to the z axis), for symmetry reasons the two components of each π orbital have the same behavior as they are degenerate. For the lower laser intensity $I_o = 3.5 \times 10^{14}$ W/cm^2, one sees that the highest occupied molecular orbital (HOMO) shows as expected the dominant response to the laser field. It is followed, respectively, by the inner-shell orbitals $3\sigma/3\sigma_u$ (HOMO-1 for OCS and HOMO-2 for CS_2, respectively). As the laser intensity increases, it emerges that the HOMO does not remain the most affected by the external laser field. Instead, our DFT/LB94 calculation shows that the ionization of the inner $3\sigma/3\sigma_u$ molecular orbital dominates so that it exceeds that of the HOMO and, thus, can become the dominant response to the field. This behavior of the π antibonding HOMOs under high laser intensity is related to their symmetry, which has a nodal plane containing the molecular axis. This gives rise to a low ionization yield when aligned parallel to the laser electric

*andre.bandrauk@usherbrooke.ca

TABLE I. Computed total ionization yield (%) γ (t_f) Eq. (2) for selected values of θ and laser intensities. Values are given in percentages.

	$I_o = 3.5 \times 10^{14}$ W/cm^2			$I = 1.4\times10^{15}$ W/cm^2		
θ	0°	45°	90°	0°	45°	90°
CS_2	5.5	6.3	4.9	8.8	10.8	6.3
OCS	2.9	3.2	2.7	6.1	7.2	5.2

field, while the $3\sigma_u/3\sigma$ MO (for OCS and CS_2, respectively) has the right symmetry (MO shape) to interact with the laser field as its density is maximum parallel to the field. One notes also that the ionization of the inner bonding $1\pi_u/1\pi$ MO is increasing with the laser intensity. At angles $\theta = 45°$ and 90°, the symmetry behavior of the different components of the π orbital is broken (degeneracy is removed) and we have renamed them as following: components of the $1\pi_g$ of CS_2 are $1\pi_g x$, $1\pi_g y$ and those of the $1\ \pi$ of the OCS are $1\pi x$, $1\ \pi y$ perpendicular to the molecular z axis. When $\theta = 45°$, independently of the laser intensity applied on the two molecules, evidence of the ionization enhancement (compare to $\theta = 0°$ case) of the HOMO is clearly visible for the two molecules. The high ionization of the HOMO is followed by that of the inner $1\pi_u/1\pi$ and $3\sigma_u/3\sigma$ MO orbitals. The enhanced ionization of the HOMO is the result of the additional effects of its lower IP and its alignment along the laser polarization axis at $\theta = 45°$ as found earlier for the one electron H_2^+ [13]. The total orbital ionization yield is found to be higher for CS_2 than for OCS. Finally, when $\theta = 90°$, once again, one finds that the KS MOs of CS_2 ionize more than that of OCS. One finds also that independently of the laser intensity, the HOMO remains the most affected by the field. For the high laser peak intensities 1.4×10^{15} W/cm^2, a net difference is noticeable on the inner KS MOs ionization behavior of the two molecules. For the CS_2 case [Fig. 2(a)], the ionization rate of the $1\pi_g y$ component of the HOMO is followed by that of the inner bonding $1\ \pi_u y$ component of the HOMO-1. At high laser intensity, the ionization rate of the $1\pi_u y$ gets closer to that of the HOMO $1\pi_g y$ because its density is maximal along the laser polarization. In the case of OCS [Fig. 2(b)], one notes by comparison with the CS_2 case that, as the laser is increasing,

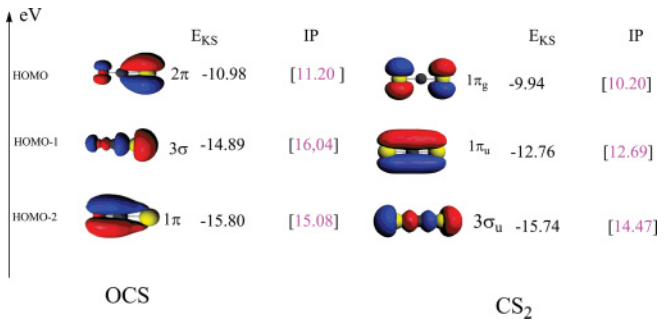

FIG. 1. (Color online) DFT/LB94 images of the KS molecular orbitals of OCS and CS_2. Only the three highest relevant occupied molecular orbitals, HOMO, HOMO-1, and HOMO-2, are shown with their energy E_{KS} and ionization potential IP (in the brackets). Equilibrium geometries parameters have been used.

the two components of the HOMO ($2\pi y$, $2\pi x$) present the dominant response to the laser field. This is because the HOMO and the HOMO-2 of the OCS have almost the same shape (density), therefore, the HOMO ionizes faster due to its lower IP.

In conclusion, we find that the KS HOMO ionization increases for both the OCS and CS_2 from $\theta = 0°$ and reaches a maximum when the molecule is aligned at an angle around 45° with respect to the direction of the laser polarization (along the z axis), and then decreases at larger angles towards 90°. To see how the molecular orientation as well as each KS orbital contributes to the total molecular ionization, we display in Table I the total molecular ionization yield [see Eq. (2)] as a function of the laser intensity and molecular orientation θ.

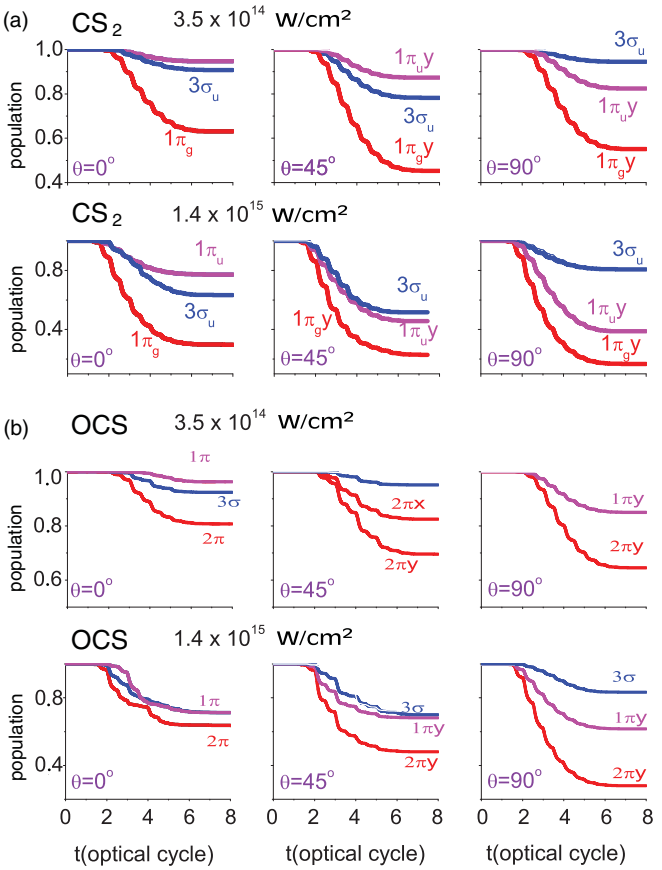

FIG. 2. (Color online) Orbital population $N_{i,\sigma}(t)$ of CS_2 and OCS at different laser intensities and for fixed angles θ between the molecular z axis and the laser polarization direction. Only the relevant KS orbitals that possess an important response to the laser field are shown with their label.

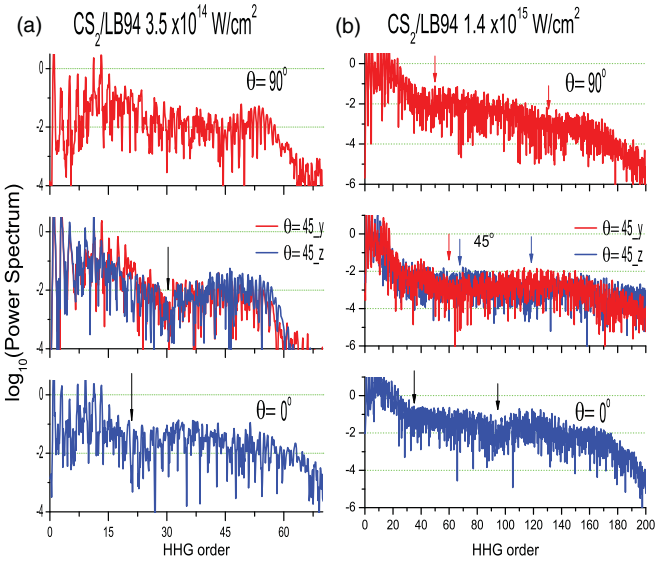

FIG. 3. (Color online) MHOHG spectra of CS_2 for fixed angles $\theta = 0°$, 45°, and 90° between the molecular z axis and the laser polarization direction. Laser pulse duration, eight optical cycles, peak intensity $I_o = 3.5 \times 10^{14}$ (a) and 1.4×10^{15} W/cm^2 (b) and wavelength 800 nm. Minima are shown by arrows.

In general, the CS_2 ionizes more than the OCS molecule due to its lower IP. The ionization is significantly enhanced at higher laser intensity in the case $\theta = 0°$ than the case of $\theta = 90°$. This is attributed to the KS MO geometry of the linear molecule. In fact, at $\theta = 0°$, the molecular ionization yield is high due to the fact that the two components of the HOMO behave in the same manner (same ionization rate) and due to the additive contribution played by the inner $3\sigma_u/3\sigma$ MO, the densities of which are aligned along the laser polarization axis, whereas for $\theta = 90°$, only one component of the HOMO as well as HOMO-2 is very active in the presence of the laser field.

We have illustrated above the importance of inner-orbital (inner-shell) ionization as laser intensities are increased [Figs. 2(a) and 2(b)]. This inner-orbital ionization first identified in C_2H_4 [14] and N_2 [15] has been recently explored to confirm interferences in MHOHG of N_2 [12,16,17] and CO_2 [18]. Examination of the MHOHG spectral intensities of CS_2 at $I = 3.5 \times 10^{14}$ W/cm^2 and $I = 1.4 \times 10^{15}$ W/cm^2 [Figs. 3(a) and 3(b)] shows for parallel orientation $\theta = 0°$ a minimum at harmonic orders $N \approx 21$, $N \approx 31$. For $\theta = 45°$, the y and z components (perpendicular and parallel to the molecular axis) of the MHOHG spectral have the same shape and a minimum is observed near the harmonic order $N \approx 31$. When the laser polarization is perpendicular to the molecular z axis $\theta = 90°$, a more diffuse spectrum is obtained. The symmetric CS_2 as for CO_2 can be treated as a two-center ionization and recombination system with emitter interference for one photon recombination [11,19–24] due to recollision of the ionized electron. An important factor in describing the recollision (recombination) amplitude is the gauge formulation, which, due to approximations in the strong-field approximations (SFA) [23], gives inequivalent recombination amplitudes in different gauges [11,19,25]. We use in this work the acceleration gauge Eq. (3), which provides the most consistent comparison with one electron TDSE numerical result [11,12]. Thus, for sums of atomic orbitals, bonding molecular orbitals of symmetry σ_g and π_u, both ionization and recombination amplitudes [12,25] will have two-center interference pattern modulations proportional to $\cos(\mathbf{p}_e.\mathbf{R}/2)$ whereas antibonding antisymmetric atomic orbital combinations of symmetry σ_u and π_g produce a $\sin(\mathbf{p}_e.\mathbf{R}/2)$ interference for electron momentum $p_e = 2\pi/\lambda_e$ (a.u.) at internuclear distance R. In Fig. 3(a), we present the MHOHG spectra for the symmetric CS_2 where electron recombination is expected to occur to the antibonding π_g HOMO as illustrated in Fig. 1. Maximum MHOHG intensities should therefore be generated for electron momentum p_e parallel to R, i.e., $\theta = 0°$. Figure 3(a) shows the MHOHG at the lowest laser intensity $I = 3.5 \times 10^{14}$ W/cm^2. A clear minimum occurs for $\theta = 0°$ at harmonic order $N \approx 21$ for which the recombining electron momentum $p_e = (2N\omega)^{1/2} = 1.62$ a.u. corresponding to a wavelength $\lambda_e = 0.2$ nm. At $\theta = 45°$, where the ionization is maximum due to the symmetry of the orbital (Table I), the minimum is shifted to larger harmonic order $N \approx 30$, for which $p_e = 1.84$ a.u. and $\lambda_e = 0.18$ nm. The effective recombination wavelength is now $\lambda_e/\sqrt{2} = 0.13$ nm. The latter satisfies approximately the destructive interference criteria $\sin(\pi R/\lambda_e\sqrt{2}) \approx 0$ since $R = 2R_{CS} = 0.31$ nm. Finally, at $\theta = 90°$, a broad spectrum is obtained with no significant minimum as compared to the $\theta = 45°$ orientation where a decrease by three orders of magnitude is observed in the MHOHG intensities at $N \approx 30$. At the higher intensity $I = 1.4 \times 10^{15}$ W/cm^2 [Fig. 3(b)], minima occur for parallel orientation $\theta = 0°$, at orders $N \approx 35, 95$. The corresponding recombination electron wavelengths are $\lambda_e = 0.17$ and 0.10 nm, thus satisfying again the destructive interference criterion $\sin(\pi R/\lambda_e) \approx 0$. At $\theta = 45°$, the separate field components E_z and E_y behave differently. The E_z component parallel to the molecular axis exhibits three minima at orders $N \approx 30$, 60, and 115, whereas the E_y component has no minimum but rather a maximum at $I = 1.4 \times 10^{15}$ W/cm^2 at $N \approx 115$. The E_z minima correspond to effective electron recombination wavelengths $\lambda_e/\sqrt{2} = 0.13$, 0.1, and 0.06 nm, thus satisfying the destructive interference criterion for centrosymmetric π_g orbitals $\sin(\pi R/\lambda_e\sqrt{2}) \approx 0$. The maximum in E_y at $N \approx 115$ suggests contribution from the bonding HOMO-1, i.e., the π_u orbital for which $\cos(\pi R/\lambda_e\sqrt{2}) \approx 1$, and its ionization rate is 50% of the π_g HOMO. This result should be measurable as elliptically polarized harmonics around $N = 115$.

Figure 4 illustrates the MHOHG spectra of the nonsymmetric OCS at intensities $I = 3.5 \times 10^{14}$ W/cm^2 [Fig. 4(a)] and 1.4×10^{15} W/cm^2 [Fig. 4(b)]. As illustrated in Fig. 1, the 2π HOMO is now mainly concentrated at the O and the S atoms with a node at C with total internuclear distance $R_{OS} = 0.27$ nm. At the lower intensity $I = 3.5 \times 10^{14}$ W/cm^2 [Fig. 4(a)], one observes two minima in the MHOHG spectrum at harmonic order $N = 15$ and 37. The corresponding recombining electron wavelengths are $\lambda_e = 0.26$ and 0.16 nm, corresponding to R and $R/2$ in OCS. This satisfies the maximum interference (minimum intensity)

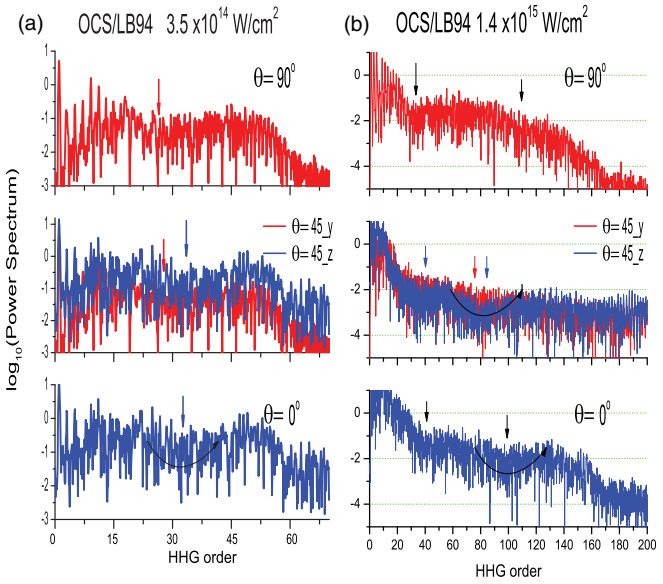

FIG. 4. (Color online) MHOHG spectra of OCS for fixed angles $\theta = 0^\circ$, 45°, and 90° between the molecular axis and the laser polarization direction. Laser pulse duration, eight optical cycles, peak intensity $I_o = 3.5 \times 10^{14}$ (a) and 1.4×10^{15} W/cm^2 (b). Minima are shown by arrows.

criteria $\sin(\pi R/\lambda_e) \approx 0$. Clearly, the density node in the OCS 2π HOMO at the C atom, which results in the phase change at the O and the S atoms, is a major consequence of the negative interference in the recombination amplitude. At 90°, where negligible interference is expected since $\mathbf{p}_e$ is perpendicular to $\mathbf{R}$, a slight minimum is observed at N ≈ 25, reflecting perhaps the neglect of field corrections to both continuum and bound-electron wave functions since electron recombination at low harmonic order generally occurs in the nonzero field for multicenter systems [11,12]. This minimum at 90° is intensified and shifted to higher order $N \approx 30$ at the higher intensity 1.4×10^{15} W/cm^2, whereas for the parallel configuration $\theta = 0^\circ$, two minima occur at $N \approx 40$ with $\lambda_e = 0.16$ nm and at $N = 100$ with $\lambda_e = 0.1$ nm, which again correspond approximately to $R/2$ and $R/3$, thus satisfying approximately the simple rule $\sin(\pi R/\lambda_e) \approx 0$ for minimum intensity due to two-center interference. We note that, at $\theta = 45^\circ$ in Fig. 4(b) for OCS, the E_z and E_y field components of harmonics behave differently compared to CS_2 [Fig. 3(b)]. The E_z component in OCS has two identifiable minima at $N = 40$ and 80 with effective recombination wavelengths $\lambda_e/\sqrt{2} = 0.11$ and 0.08 nm satisfying the destructive interference rule $\sin(\pi R/\lambda_e\sqrt{2}) \approx 0$. The E_y component of OCS has no clearly discernible minimum as compared to CS_2 [Fig. 3(b)], where a minimum in the E_z component at $N \approx 115$ becomes a maximum in the E_y component. In CS_2, this is attributed to an increasing contribution of the bonding π_u HOMO-1 [Fig. 2(a)], resulting to an enhancement of elliptically polarized harmonics [26].

The nonlinear nonperturbative TDDFT calculations presented in this paper for symmetric CS_2 and nonsymmetric OCS tri-atoms address MHOHG occurring from MO ionization at high laser intensities. The results reveal a strong dependence on molecular orientation and laser intensities. In general, MHOHG with the highest signal intensities are obtained when the laser polarization axis is along a major axis of electron density in the MOs, and those with the lowest signal intensities occur when the laser polarization axis is parallel with a nodal plane in the MO. The difference in the MHOHG spectrum of the two molecules between the orientation $\theta = 90^\circ$ and 0° is found arising from the ionization of inner-shell MOs and the nature of the two nuclei in the presence of the laser field. In fact, for CS_2, two sulfur nuclei experience differently the laser field (potential energy difference) at $\theta = 0^\circ$, whereas at $\theta = 90^\circ$, they experience the same tunneling ionization and the resulting wave packets are driven by the laser, thus, not leading to significant destructive interference. For OCS, the HOMO located on the oxygen and the sulfur nuclei behaves as in CS_2 for $\theta = 0^\circ$, whereas at $\theta = 90^\circ$, the two nuclei experience a different tunneling ionization due to their electronegativity difference. Ionization is found higher for CS_2 than for OCS due to their IP difference. In addition, molecular ionization is found lower when the molecular axis is perpendicular to the laser-electric-field polarization as compared to the parallel case for the molecules CS_2 in agreement with single continuum-bound recombination amplitude in the acceleration gauge. Furthermore, the MHOHG spectra show in the plateau region at different molecular orientation that intensity of harmonics can be weak. In general, for intensities above $I = 3.5 \times 10^{14}$ W/cm^2, inner-shell orbitals, i.e., lower highest occupied molecular orbitals (HOMO-1 and HOMO-2) with larger ionization potentials than the highest occupied orbital (HOMO) can contribute considerably to total ionization. The main reason is that these inner-valence orbitals have fewer nodes than the HOMO and, therefore, for certain laser polarization, the density of these lower (but higher IP) orbitals at the laser-molecule angle θ is much larger than the HOMO. At angle $\theta = 45^\circ$, the degeneracy of π orbitals is removed by the laser, resulting in different MHOHG polarization components E_y and E_z. This should result in enhanced elliptically polarized harmonics. As a general rule, we note that the ionization is generally enhanced as the molecule is aligned along the major axis of the electron distribution in the active molecular orbital. It should be emphasized that, while the LB94 potential in the present TDDFT calculation yields good molecular orbital ionization potentials IP, further study of MHOHG including the nuclear separation distance effects such as recently reported [27] for H_2 and using more accurate exchange potentials based on long-range–short-range corrected models [28,29] offer scope for future accurate characterization of MHOHG processes in large molecules. We note, finally, that OCS and CS_2 are highly polarizable molecules and require dipole and polarizability Stark corrections to tunneling [30] and SFA theories [31]. Interference between dipole and polarizabiliy effects in strong fields has been earlier suggested as a means of controlling transition states in chemical reactions [32,33]. Such nonlinear effects will depend on carrier envelope phase (CEP) for ultrashort pulses in nonsymmetric molecules [34] and offer further scope for studying MHOHG and polarization of the harmonics in multicenter molecules.

[1] E. F. Penka and A. D. Bandrauk, Phys. Rev. A **81**, 023411 (2010).
[2] C. A. Ullrich and A. D. Bandrauk, in *Time-Dependent Density Functional Theory*, edited by M. A. L. Marques *et al.* (Springer, Berlin, 2006), pp. 357–374.
[3] R. V. Leeuwen and E. J. Baerends, Phys. Rev. A **49**, 2421 (1994).
[4] M. Awasthi *et al.*, Phys. Rev. A **77**, 063403 (2008).
[5] S.-K. Son and S.-I. Chu, Chem. Phys. **91**, 366 (2009).
[6] J. V. Ortiz, Int. J. Quantum Chem. **100**, 1131 (2004).
[7] C. R. Brundle and D. W. Turner, Int. J. Mass Spectrom. Ion Phys. **1**, 285 (1968).
[8] D. W. Turner and D. P. May, J. Chem. Phys. **46**, 1156 (1967).
[9] C. R. Brundle and D. W. Turner, Int. J. Mass Spectrom. Ion Phys. **2**, 195 (1969).
[10] M. I. Al-Joboury *et al.*, J. Chem. Soc. **616**, 6350 (1965).
[11] A. D. Bandrauk *et al.*, in *Progress in Ultrafast Intense Laser Science*, edited by K. Yamanouchi *et al.*, Vol. III (Springer, Tokyo, 2006).
[12] G. L. Kamta and A. D. Bandrauk, Phys. Rev. A **71**, 053407 (2005).
[13] G. L. Kamta and A. D. Bandrauk, Phys. Rev. A **74**, 033415 (2006).
[14] A. Talebpour *et al.*, Chem. Phys. Lett. **313**, 789 (1999).
[15] A. Becker *et al.*, Chem. Phys. Lett. **343**, 345 (2001).
[16] B. K. McFarland *et al.*, Phys. Rev. A **80**, 033412 (2009).
[17] B. K. McFarland *et al.*, Science **322**, 1232 (2008).
[18] Y. Mairesse *et al.*, Phys. Rev. Lett. **104**, 213601 (2010).
[19] G. L. Kamta and A. D. Bandrauk, Phys. Rev. A **70**, 011404 (2004).
[20] T. Kanai *et al.*, Nature (London) **435**, 470 (2005).
[21] T. Kanai *et al.*, Phys. Rev. Lett. **98**, 053002 (2007).
[22] M. Lein, Phys. Rev. Lett. **94**, 053004 (2005).
[23] M. Lewenstein *et al.*, Phys. Rev. A **49**, 2117 (1994).
[24] P. Liu *et al.*, Phys. Rev. A **78**, 015802 (2008).
[25] C. C. Chirila and M. Lein, J. Phys. B: At. Mol. Phys. **39**, S437 (2006).
[26] K. J. Yuan and A. D. Bandrauk, Phys. Rev. A **80**, 063412 (2010).
[27] A. D. Bandrauk *et al.*, Phys. Rev. Lett. **101**, 153901 (2008).
[28] J. Toulouse *et al.*, Phys. Rev. A **70**, 062505 (2004).
[29] H. O. Wijewardane and C. A. Ullrich, Phys. Rev. Lett. **100**, 056404 (2008).
[30] T. Brabec *et al.*, Phys. Rev. Lett. **95**, 073001 (2005).
[31] D. Dimitrovski *et al.*, Phys. Rev. A **82**, 053404 (2010).
[32] A. D. Bandrauk *et al.*, J. Chem. Phys. **121**, 7764 (2004).
[33] M. Y. Ivanov *et al.*, Phys. Rev. A **54**, 5159 (1996).
[34] X.-B. Bian and A. D. Bandrauk, Phys. Rev. Lett. **105**, 093903 (2010).